# New Insights on the Nature of the Chemical Species Involved during the Process of Dopamine Deprotonation in Aqueous Solution: Theoretical and Experimental Study

**Silvia Corona-Avendaño,[†] Georgina Alarcón-Angeles,[†] Giselle A. Rosquete-Pina,*[,‡] Alberto Rojas-Hernández,[†] Atilano Gutierrez,[†] M. Teresa Ramírez-Silva,*[,†] Mario Romero-Romo,[‡] and Manuel Palomar-Pardavé[‡]**

*Universidad Autónoma Metropolitana-Iztapalapa, Departamento de Química, Av. San Rafael Atlixco #186, Col. Vicentina, C. P. 09340, México, D. F., and Universidad Autónoma Metropolitana-Azcapotzalco, Departamento de Materiales, Av. San Pablo #180, Col. Reynosa-Tamaulipas, C. P. 02200, México, D. F.*

*Received: June 15, 2006; In Final Form: October 27, 2006*

Due to dopamine's chemical structure and the fact that it has three p$K_a$ values, its deprotonation process, in aqueous solution, may involve different chemical species. For instance, the first deprotonation step, from the fully protonated dopamine molecule ($H_3DA^+$) to the neutral one ($H_2DA$), will result in zwitterionic species if a proton from one of the OH groups in the catechol ring is lost or into a neutral species if the proton is lost from the amino group. Given that the interaction of such a product with its environment will be quite different depending on its nature, it is very important, therefore, to have an accurate knowledge of which is the dopamine chemical species that results after each deprotonation step. In order to gain a better understanding of dopamine chemistry and to establish a plausible dopamine deprotonation pathway, the optimized geometries of the aforementioned species were calculated in this work by means of the density functionals theory (B3LYP/6-311+G(*d*,*p*)) in both cases: in vacuo and with solvent effect, to assess, among other theoretical criteria, the proton affinities of the different dopamine species. This permitted us to propose the following reaction pathway:

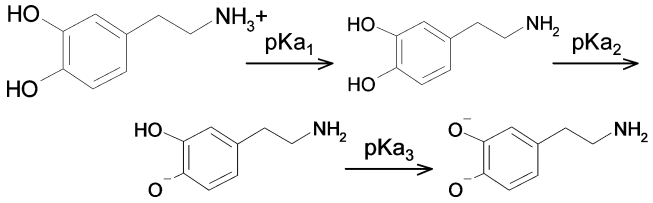


Moreover, the calculations of the chemical shift (NMR−GIAO) modeling the effect of the solvent with a continuum method (PCM) was in agreement with the $^{13}C$ NMR experimental spectra, which confirmed even further the proposed deprotonation pathway.

## 1. Introduction

Dopamine (DA) is a neurotransmitter associated with proper functioning of several organs such as the heart, brain, and suprarenal glands. Also, it has been reported that the presence of dopamine and tetrahydrobiopterin $BH_4$ constitute an important factor in rendering dopaminergic cells vulnerable, which implies that a depletion of dopamine attenuates toxicity over such cells.[1] Therefore, DA is directly related to biologically relevant aims.[2−4] Due to this, the implementation of analytical methods for DA determination that are able to offer greater certainty in the determination of dopamine concentration must be based on a clearer understanding of the chemical behavior of dopamine in aqueous solution, where pH plays a very important role.

In view of the importance granted to achieving an adequate knowledge of DA's chemical structure at different pH values, there are a number of studies which have focused on the determination of the acidity constants, p$K_a$; see Table 1. These determinations have been carried out through potentiometry and acid−base or spectrophotometry titrations.

**TABLE 1: Values of the Acidity Constants for DA Reported in the Literature**

| ref | p$K_{a_1}$ | p$K_{a_2}$ | p$K_{a_3}$ |
|---|---|---|---|
| Sánchez-Rivera et al. (5) | 9.05 | 10.58 | 12.07 |
| Gerard and Chehhal (6) | 9.05 | 10.55 | 12.81 |
| Sedeh and Ohman (7) | 8.93 | 10.49 | |
| Kiss and Martin (8) | 8.01 | 12.37 | 13.7 |
| Kiss and Gergely (9) | 8.89 | 10.41 | 13.1 |
| Kuznar and Weber (10) | 9.06 | 10.6 | 12.05 |

As seen in Table 1, there are differences among the p$K_a$ values reported that can be attributed to the diversity of experimental conditions used to evaluate the constants. However, the assessment effected by Sánchez-Rivera et al.[5] carefully considered the experimental parameters that most likely affected DA's behavior, to exert close control upon them. With these data it is possible to construct the predominance zones diagram (PZD) as a function of pH, shown in Figure 1.

From the PZD shown in Figure 1, it can be noted that there are four pH regions where each of the dopamine species in

* Corresponding authors. E-mail: mtrs218@xanum.uam.mx (M.T.R.-S.); grosquete@correo.azc.uam.mx (G.A.R.-P.).
[†] Universidad Autónoma Metropolitana-Iztapalapa.
[‡] Universidad Autónoma Metropolitana-Azcapotzalco.

10.1021/jp0637227 CCC: $37.00 
Published on Web 01/27/2007

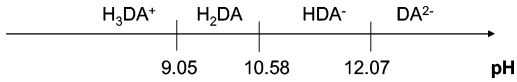


**Figure 1.** PZD of the DA species built with the p$K_a$ data reported by Sánchez-Rivera et al. (ref 5).

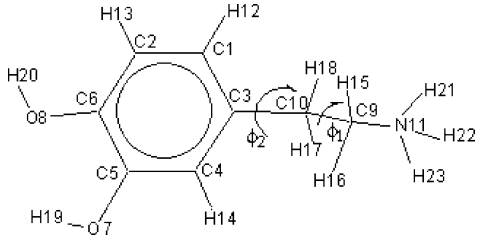


**Figure 2.** Schematic representation and atom numbering of the $H_3DA^+$ molecule. The dihedral angles $\phi_1$ and $\phi_2$ are also shown in the figure.

solution can predominate. The species formed are the fully protonated $H_3DA^+$ or cationic, the neutral species $H_2DA$, the anionic species $HDA^-$, and the completely deprotonated species, $DA^{2-}$.

The molecular structure of DA shown in Figure 2 represents the fully protonated molecule. This molecule consists of an amine group and a catechol ring. $H_3DA^+$ is the form present under the conditions imposed by the physiological pH,[4] as can be corroborated with the diagram shown in Figure 1, because the $H_3DA^+$ species predominates up to pH = 9.05. However, when the pH increases, the manner in which the protons are lost may follow a variety of deprotonation paths, which engenders problems in trying to assign each of the resulting structures to a particular p$K_a$ value.

In this regard, Kiss and Martin[8] proposed that either of the OH groups in the catechol ring loses a proton, and then the amine group follows, then last of all, the other hydroxyl of the catechol ring. However, the proposal does not clarify which of the hydroxyls becomes deprotonated first, leading to the possibility of two pathways that fulfill such a proposal; see pathways A and B in Scheme 1. Either the first hydroxyl deprotonated first, namely, the one located at C6 (pathway A), or the one located at C5 (pathway B).

As can be observed in Scheme 1, the hydroxyl group that becomes deprotonated first produces different chemical structures that are available during the deprotonation process; such differences have great biological importance, which implies that it is fundamental to determine the predominant structures under a given set of conditions.

Furthermore, some studies report p$K_a$ values for the catechol ring and the ethylene amine chain, which are shown in Table 2.

Considering the values shown in Table 2 and comparing them with the values obtained for DA,[5] one may roughly conclude that the $pK_{a_1} = 9.05$ and $pK_{a_3} = 12.07$ of DA corresponds to the deprotonation of the hydroxyls of the catechol ring, while the $pK_{a_2} = 10.58$ of DA corresponds to the ethylene amine deprotonation, which is in agreement with the pathway proposed by Kiss and Martin.[8] However, there is no evidence of which hydroxyl group of dopamine will release its proton first.

Moreover, Rajan et al.[17] proposed that the first deprotonation occurs at the amine group, while the second and third occur at

**SCHEME 1: Two Possible Deprotonation Pathways That Match the Proposed Mechanism of Kiss and Martin[a]**

Pathway A

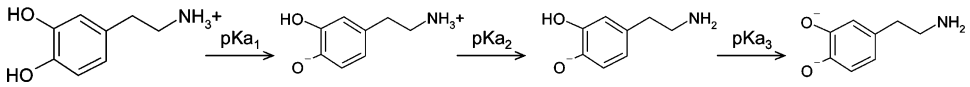


Pathway B

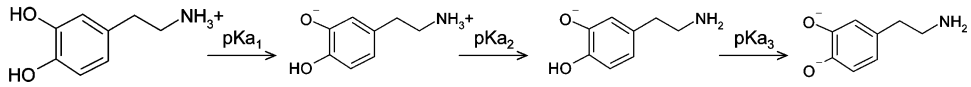


[a] Reference 8.

**SCHEME 2: Two Possible Deprotonation Pathways That Match the Proposed Mechanism of Rajan et al.[a]**

Pathway C

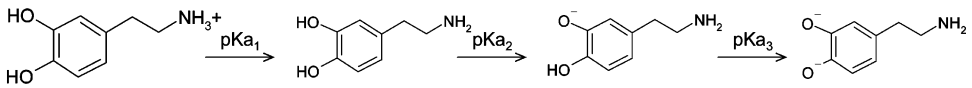


Pathway D

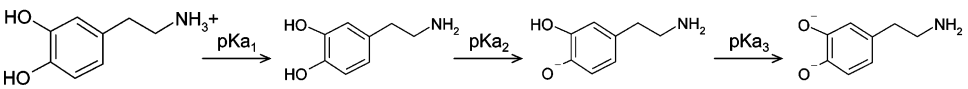


[a] Reference 17.

**TABLE 2: Acidity Constants of the Catechol Ring and of the Ethylenamine**

| catechol | | | ethylene amine | |
|---|---|---|---|---|
| p$K_{a_1}$ | p$K_{a_2}$ | ref | p$K_{a_1}$ | ref |
| 9.46 | 12.52 | Hancock and Orszulik (11) | 10.61 | Porzsolt et al. (14) |
| 8.34 | 13.66 | Manjula and Bhattacharya (12) | 10.66 | Hancock et al. (15) |
| 9.25 | 13 | Balla et al. (13) | 10.68 | Jameson et al. (16) |

**SCHEME 3: Two Remaining Deprotonation Pathways for Dopamine in Aqueous Solution**

Pathway E

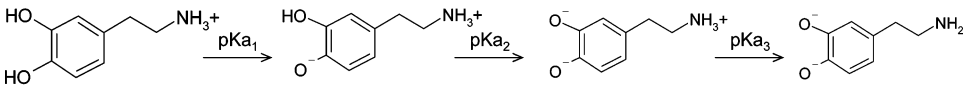


Pathway F

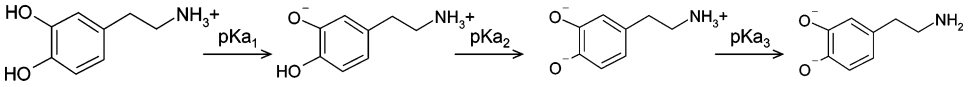


**TABLE 3: Possible Rotational Conformers Resulting from the Combination of the Dihedral Angles $\phi_1$ and $\phi_2$ in the $H_3DA^+$ Molecule**

| | anti ($\phi_1 = 180$) | | | gauche ($\phi_1 = \pm 60$) | | |
|---|---|---|---|---|---|---|
| | α ($\phi_2 = 0$) | perpendicular ($\phi_2 = 90$) | β ($\phi_2 = 180$) | α ($\phi_2 = 0$) | perpendicular ($\phi_2 = 90$) | β ($\phi_2 = 180$) |
| ($\phi_1$, $\phi_2$) (deg) | 180, 0 | 180, 90 | 180, 180 | +60, 0<br>−60, 0 | +60, 90<br>−60, 90 | +60, 180<br>−60, 180 |

**TABLE 4: Variation of the Total Energies (B3LYP/6-311+G(*d*,*p*)/PCM), Chemical Potential ($\mu$), and Chemical Hardness ($\eta$) Calculated with the B3LYP/6-311+G(*d*,*p*)/PCM Geometry at MP2/6-311+g(*d*,*p*) and AM1 Level for the Three Rotamers of DA**

| | $\Delta E$ (kcal/mol) | $\mu$ (eV) | | $\eta$ (eV) | |
|---|---|---|---|---|---|
| rotamers | B3LYP/6-311+G(*d*,*p*)/PCM | MP2/6-311+g(*d*,*p*) | AM1 | MP2/6-311+g(*d*,*p*) | AM1 |
| anti | −0.26 | −7.03 | −7.94 | 8.44 | 7.31 |
| distal | −0.09 | −7.11 | −8.04 | 9.03 | 7.79 |
| proximal | 0 | −7.08 | −8.04 | 9.03 | 7.82 |

**TABLE 5: Proton Affinities (PA) of the Neutral Species $H_2DA$-I, $H_2DA$-II, and $H_2DA$-III, Forming $H_3DA^+$, Calculated by B3LYP/6-311+G(*d*,*p*)/PCM According to Eq 1**

| | PA (B3LYP/6-311+G(*d*,*p*)/PCM) (kcal/mol) | ΔPA (B3LYP/6-311+G(*d*,*p*)/PCM) (kcal/mol) |
|---|---|---|
| $H_2DA\text{-I} + H^+ \rightarrow H_3DA^+$ | 283.644 | 0 |
| $H_2DA\text{-II} + H^+ \rightarrow H_3DA^+$ | 294.749 | 11.105 |
| $H_2DA\text{-III} + H^+ \rightarrow H_3DA^+$ | 291.328 | 7.684 |

the hydroxyl groups in the catechol ring; see Scheme 2. The present proposal is different with respect to that of Kiss and Martin.[8] However, it should be remarked again that it is not indicated which of the OH groups will be the first to contribute to the ongoing deprotonation; this fact brings in two pathways (see Scheme 2) that match Rajan et al.'s proposal.

In 1994, Gerard and Chehhal[6] assumed, without any experimental or theoretical evidence, that the first deprotonation corresponded to the OH group, bound to C5, followed by the amine group, bound to C9, and finally the deprotonation of the second OH group of the catechol ring, bound to C6. It is possible to note that this sequence is in agreement with that proposed by Kiss and Martin,[8] following pathway B in Scheme 1.

As can be noted, the possible pathways for dopamine deprotonation are not many. Aside from those already suggested by Kiss and Martin, see Scheme 1, and Rajan et al., see Scheme 2, there are only two more possibilities; see Scheme 3. Therefore, in this study we will consider all the possibilities to asses the more plausible path for dopamine deprotonation and also the possibility of interception among them.

It is pertinent to mention that, for quite some time now, theoretical studies have become essentially useful to gain a better understanding on the behavior of DA,[18−26] even if some of the papers referred exhibited somewhat obsolete methods.[18−21] The majority of the computational studies of DA that have been developed are related to its conformational properties in the gaseous phase[23−25] and also in the presence of solvent.[23,25,26] Some of the species that result from DA's deprotonation processes[25] have been studied. However, up to this moment, there is not a detailed study on the molecular structures of all the isomers resulting from proton losses (see Schemes 1−3) and their proton affinities which may become directly related to a set of properties derived from pH changes.

With the previous considerations in mind, it becomes important to establish as exactly as possible the relative order in which the deprotonation process of DA takes place. This way, the prevailing structure at each pH interval will be known so that it becomes possible to determine the interactions with different types of molecules of organic compounds or metals that are likely to appear in the system under scrutiny.

On the basis of the aforementioned, the aim of the present investigation is to find and corroborate the most likely order in which DA becomes deprotonated, with particular reference to all pathways that can be followed. Therefore, using the density functionals theory, DFT, it was thought appropriate to perform theoretical calculations of the chemical shift by nuclear magnetic resonance−gauge including atomic orbital (NMR−GIAO) and modeling the solvent effect with a continuum method, namely, the polarizable continuum model (PCM). The results obtained were experimentally corroborated by means of nuclear magnetic resonance analysis, $^{13}C$ NMR.

## 2. Theoretical Method

Overall geometry optimizations and frequency calculations with DFT[27] were carried out, specifically with the Becke3LYP

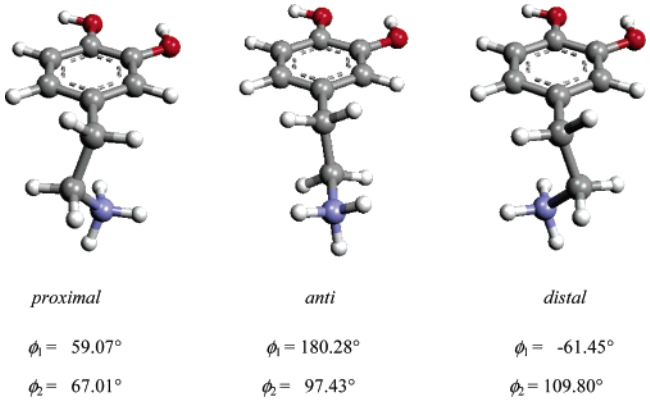


**Figure 3.** DFT (B3LYP/6-311+G(*d*,*p*)/PCM) optimized geometries of the most stable rotamers of DA: dihedral angles $\phi_1$ and $\phi_2$.

functional[28] and the basis set 6-311+G(*d*,*p*) for both cases: in vacuo and with solvent effect. The polarizable continuum model (PCM) of Miertus et al.[29] was employed using the united atom topological model[30] to build the cavity with the following features: GePol (Rmin = 0.2 Ofac = 0.890), default sphere (NSphG = 11), tesserae with average area of 0.2 Å$^2$.

Thermal energies were simultaneously computed, and both the $\Delta H_{298}$ for the protonation reaction and the proton affinity (PA) were determined using eq 1:[31]

$$\mathrm{PA} = -\Delta H_{298} = \Delta E_0 + \Delta E_{\mathrm{therm}} \qquad (1)$$

where $\Delta E_0$ is the difference in the total energies of the species at 0 K and $\Delta E_{\mathrm{therm}}$ includes contributions from zero-point vibrational energy differences, thermal vibrational energy differences, rotational energy differences, and thermal translational energy differences.

The frontier orbital corresponding to the lowest unoccupied molecular orbital (LUMO) was calculated by the semiempirical method AM1.[32]

GIAO was employed[33] to calculate the theoretical NMR spectrum using the same functional and basis as those for the geometry optimizations. Then, using GaussView 3.0, the calculated magnetic shielding tensors (chemical shifts) were referred to $(CH_3)_4Si$ (TMS), considering its values obtained at B3LYP/6-311+G(2*d*,*p*)-GIAO. To study the effect of the solvent in the theoretical NMR spectra, a water continuum was modeled with the PCM method.[29] For all cases, Gaussian 2003[34] was used. Also, to visualize the molecules and the theoretical NMR spectra, GaussView 3.0[35] was used. Argus Lab[36] was used to calculate (AM1) and visualize the LUMO density surface of the different protonated forms of dopamine.

To assess their properties and the theoretical spectra, a Dell Precision 670, 2 CPU Xeon 2.8 GHz, 2 Gb RAM, 256 HD and a PC Dell Dimension 8400, CPU Pentium 4.3 GHz, 1 Gb RAM, 128 Gb HD were used.

## 3. Experimental Section

The DA stock solution was prepared from reagent grade A R Merck substance and, to adjust the pH of the solutions, NaOH (99% purity) or HCl (37%), also from Merck, were used. The spectra were obtained by means of a Bruker AMX 500 NMR spectrometer, using deuterated water, $D_2O$, as solvent and 2,2-dimethyl-2-silapentane-5-sulfonate sodium (DSS) as reference. The solution pH was measured by means of a combined micro-pH glass electrode (Metrohm).

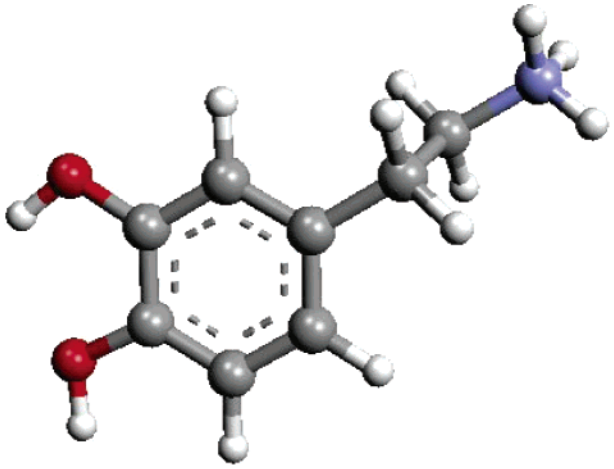

**Figure 4.** Minimal energy geometry (B3LYP/6-311+G(*d*,*p*)/PCM) of N-protonated dopamine (anti).

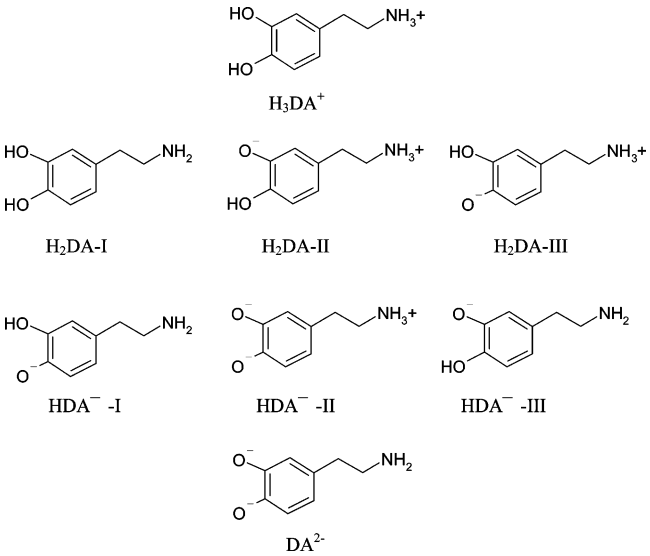


**Figure 5.** Species involved during the deprotonation process of N-protonated dopamine ($H_3DA^+$).

**TABLE 6: Relative Molecular Energies ($\Delta E$) (B3LYP/6-311+G(*d*,*p*)/PCM for the Different Isomers Resulting from the Deprotonation of $H_3DA^+$: $H_2DA$-I, $H_2DA$-II, $H_2DA$-III**

| relative molecular energies ($\Delta E$) (B3LYP/6-311+G(*d*,*p*)/PCM) (kcal/mol) | | |
|---|---|---|
| $H_2DA$-I | $H_2DA$-II | $H_2DA$-III |
| −10.12 | −3.63 | 0 |

## 4. Results and Discussion

**4.1. Theoretical Study of Dopamine.** *4.1.1. Conformers of N-Protonated Dopamine.* The theoretical studies reported so far on dopamine are mostly conformational because of the several different structures that the compound is capable of generating. Strictly on consideration of the combination of angles $\phi_1$ and $\phi_2$, as indicated in Table 3, nine different structures result if the following angles are used as model ± (0, 60, 90, 180), that is, without taking into account those others that would result if the spatial position of the hydrogen atoms (H) in the OH groups were considered. It is basically relevant to take into account the structure−activity relationship in the context of biological phenomena. For such matters, the theoretical calculations have contributed quite clear elucidations to establish such relations.

It has been demonstrated through rotational profiles AM1, either of the gas phase or the aqueous solution, AM1/SM1 with

**TABLE 7: Proton Affinities (PA) of the Species HDA⁻-I and HDS⁻-III, Forming $H_2$DA-I, Calculated by B3LYP/6-311+G(*d,p*)/PCM According to Eq 1**

| | PA (B3LYP/6-311+G(*d*,p)/PCM) (kcal/mol) | ΔPA (B3LYP/6-311+G(*d,p*)/PCM) (kcal/mol) |
|---|---|---|
| HAD⁻-I + $H^+ \rightarrow H_2$DA-I | 288.722 | 0 |
| HAD⁻-III + $H^+ \rightarrow H_2$DA-I | 292.050 | 3.328 |

**TABLE 8: Relative Molecular Energies (Δ*E*) (B3LYP/6-311+G(*d,p*)/PCM for the Different Isomers Involved during Deprotonation of $H_2$DA-I According to Pathway C (HDA⁻-III) and D (HDA⁻-I)**

| relative molecular energies (Δ*E*) (B3LYP/6-311+G(*d,p*)/PCM) (kcal/mol) | |
|---|---|
| HAD⁻-I | HAD⁻-III |
| −3.571 | 0 |

AMSOL, that the conformations with a dihedral angle $\phi_2 = 90$, namely, the perpendicular conformations, are the most stable ones.[25] Amidst these three, the two gauche-perpendicular (+60, 90) and (−60, 90) have much smaller energies, almost equal among themselves, than the anti-perpendicular (180, 90), though there seems to be a slight preference for the gauche-perpendicular corresponding to +60, 90. Calculations QCISD-(T)/6-31G*//HF/6-31G* and MP2/6-311++G**//MP2/6-311++G** based on optimizations DFT B3LYP/6-31G*[23] and HF/6-31G confirm so.[23] However, when using the solvation model AM1/SM1, it has been found that the anti-perpendicular conformation brings an important contribution to the N-protonated dopamine.[25]

Figure 3 shows the molecular geometries obtained with the total DFT optimization, DFT (B3LYP/6-311+G(*d,p*)/PCM), of the three perpendicular conformations of N-protonated DA: from now on the anti-perpendicular will be denoted as anti, and in order to differentiate the gauche-perpendicular, one will be called *distal* and the other *proximal*. The figure also includes the dihedral angles $\phi_1$ and $\phi_2$ obtained with the total DFT optimization.

Table 4 shows the relative energies B3LYP/6-311+G(*d,p*)/PCM of the rotamers as well as the values of the chemical potential $\mu$ and the chemical hardness $\eta$, calculated with the energies of the frontier orbitals AM1 and MP2 using the concepts of DFT as follows:

The chemical potential ($\mu$) and the chemical hardness ($\eta$) are defined as

$$\mu = \left[\frac{\partial E}{\partial N}\right]_{v(r)} \tag{2}$$

$$\eta = \left[\frac{\partial^2 E}{\partial N^2}\right]_{v(r)} \tag{3}$$

where $E$ is the total energy, $N$ is the total number of electrons, and $v(r)$ is the external potential generated by the nuclei.

The finite difference approximation leads to the operational definition of absolute or chemical hardness as

$$\eta \cong I - A \tag{4}$$

and of chemical potential ($\mu$):

$$\mu \cong -\frac{(I + A)}{2} \tag{5}$$

where $I$ is the ionization potential and $A$ is the electron affinity. Within the validity of Koopman's theorem, the frontier orbital energies are given by eqs 6 and 7

$$-\epsilon_{HOMO} \cong I \tag{6}$$

$$-\epsilon_{LUMO} \cong A \tag{7}$$

Therefore, $\eta$ corresponds to the difference between the energies of the highest occupied molecular orbital (HOMO) and the lowest unoccupied molecular orbital (LUMO).

These results show that the lowest energy corresponds to the anti rotamer. From the previous results it becomes possible to conclude that the anti rotamer, namely, the anti-perpendicular (180, 90), is the most stable structure, which is in agreement with published results.[23,25] Once the optimum geometry of the N-protonated dopamine (see Figure 4) has been defined, a theoretical study was carried out to determine the deprotonation order, following different criteria, namely, PA, more stable dopamine species, atomic charge (Mulliken), bond length, and LUMO density surface location.

*4.1.2. Theoretical Study of the Deprotonation Order of N-Protonated Dopamine.* In order to analyze the dopamine deprotonation order, the following calculations were done for all the different dopamine chemical species shown in Schemes 1−3. Calculations were performed for all the species shown in Figure 5 using the same theory level as that used for the study of the N-protonated dopamine. It is important to point out that for this study we used the anti rotamer optimized geometry, considering solvent effect, as the fully protonated dopamine ($H_3$-DA⁺).

As can be appreciated, after the first and second deprotonation the resulting species will be $H_2$DA and HDA⁻, respectively. For each of them there exist three isomers, namely, $H_2$DA-I, $H_2$DA-II, and $H_2$DA-III for $H_2$DA and HDA⁻-I, HDA⁻-II, and HDA⁻-III for HDA⁻; see Figure 5.

After total geometry optimization and frequency analysis for the eight dopamine species in Figure 5, the results obtained will be discussed in the following sections. It is important to stress that the DA deprotonation pathways shown in Schemes 1−3 could be intercepted if one considered the possibility of interconversion between $H_2$DA-II and $H_2$DA-III as well as HDA⁻-I and HDA⁻-III by proton exchange (intramolecular or solvent-assisted) to lead to the respective isomeric species according to reactions 8 and 9, respectively:

$$H_2\text{DA-II} \rightleftarrows H_2\text{DA-III} \tag{8}$$

$$\text{HDA}^-\text{-I} \rightleftarrows \text{HDA}^-\text{-III} \tag{9}$$

Thus, in the following discussion we are going to analyze the deprotonation pathway of the totally protonated dopamine ($H_3DA^+$), taking into account the possibility of interconversion between the two isomers that are possible for each species containing a singly deprotonated catechol group that may result in interception of the different pathways considered in this paper, namely, A with B, C with D, and E with F.

4.1.2.1. Proton Affinity (PA) and Relative Stability of Isomers. Table 5 shows the proton affinities of three isomers ($H_2$DA-I, $H_2$DA-II, and $H_2$DA-III) corresponding to the three different possibilities for the first deprotonation of the fully protonated dopamine molecule, $H_3DA^+$ (see Figure 5). It is

**TABLE 9: Proton Affinities (PA) of $DA^{2-}$ to Form $HDA^{-}$-I or $HDA^{-}$-III Calculated by B3LYP/6-311+G(*d,p*)/PCM According to Eq 1**

| | PA (B3LYP/6-311+G(*d,p*)/PCM) (kcal/mol) | PA (B3LYP/6-311+G(*d,p*)/PCM) (kcal/mol) |
|---|---|---|
| $DA^{2-} + H^{+} \rightarrow HAD^{-}$-I | 308.333 | 0 |
| $DA^{2-} + H^{+} \rightarrow HAD^{-}$-III | 305.005 | 3.328 |

**TABLE 10: Selected Mulliken Atomic Charges (B3LYP/6-311+G(*d,p*)/PCM) of N-Protonated Dopamine ($H_3DA^{+}$)**

| Mulliken atomic charges (B3LYP/6-311+G(*d,p*)/PCM | |
|---|---|
| | $H_3DA^{+}$ |
| H19 | 0.330 |
| H20 | 0.353 |
| H21 | 0.374 |
| H22 | 0.364 |
| H23 | 0.364 |

**TABLE 11: Selected Bond Distances (angstrom) B3LYP/6-311+G(*d,p*)/PCM of N-Protonated Dopamine ($H_3DA^{+}$)**

| bond distances (angstrom) B3LYP/6-311+G(*d,p*)/PCM | |
|---|---|
| | $H_3DA^{+}$ |
| O7−H19 | 0.977 |
| O8−H20 | 0.983 |
| N11−H21 | 1.032 |
| N11−H22 | 1.033 |
| N11−H23 | 1.033 |

important to mention that, recently, similar calculations were done theoretically by Gómez et al.[39] for 2-pyridy-azolez. From Tables 5 and 6 it is possible to note that the species with the lower PA value and relative molecular energy is $H_2DA$-I. Consequently, this indicates that the most probable molecule to be formed after the first deprotonation of $H_3DA^{+}$ would be $H_2DA$-I, thereby making pathways A, B, E, and F less energetically favorable than pathways D and C. Then, it seems that reaction 8 is not feasible. Therefore, these last two deprotonation pathways would be the only remaining possibilities for $H_3DA^{+}$.

In order to identify which pathway (D or C) is the most favorable one then, once again, we analyzed the PA and relative molecular energies of the molecules involved during the deprotonation of $H_2DA$-I. From Tables 7 and 8 it is noteworthy that $HDA^{-}$-I has lower relative energy and lower PA than $HDA^{-}$-III; therefore, the lowest energy pathway corresponds to D. It is important to note that interconversion between $HDA^{-}$-I and $HDA^{-}$-III molecules (see reaction 9) is an energetically unfavorable reaction by about 3.6 kcal/mol (see Table 6).

Moreover, if we analyze the PA of the completely deprotonated dopamine molecules ($DA^{2-}$) (see Table 9) the same outcome can be reached regarding D as the most stable pathway. From this discussion, it is relevant to mention that interconversion between intermediate species during this process is not energetically favorable. Notwithstanding, the energy difference between $HDA^{-}$-I and $HDA^{-}$-III cannot be considered large enough to definitely neglect the possibility of interconversion (see reaction 9); thus, if this is to happen, pathways D and C would intercept.

In order to provide further theoretical support to our main outcome obtained by thermodynamic parameters such as PA and relative energy, we will analyze in the following section the lability of the chemical bond associated with the acid protons in the DA molecule through features such as Mulliken charges, bond distances, and LUMO density surface calculated in these molecules.

4.1.2.2. Total Atomic Charges (Mulliken) and Interatomic Bond Distances. Table 10 shows Mulliken atomic charges (B3LYP/6-311+G(*d,p*)/PCM) corresponding to the H atoms associated to the amino group (H21,H22, and H23) and those associated to the oxygen atoms of the catechol ring (H19 and H20) of the N-protonated dopamine ($H_3DA^{+}$). From Table 10, it becomes possible to appreciate that the more positive values of the Mulliken charge correspond to the amine group's hydrogen atoms. Thus, this indicates that the said H atoms would be more likely the first ones to be lost during deprotonation. Furthermore, this can also be confirmed from the data presented in Table 11, related with the bond distances of the groups associated with the deprotonation. These analyses further support the idea that the N-protonated dopamine ($H_3DA^{+}$) deprotonation process ($pK_{a_1}$) must start with the following reaction 10:

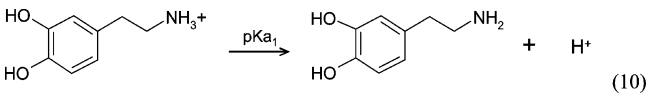


(10)

As can be noted this corresponds to the first reaction in pathways C or D.

4.1.2.3. Lowest Unoccupied Molecular Orbital Density Surface. Figure 6 displays the graphic form of the LUMO of the $H_3DA^{+}$, $H_2DA$-I, and $HDA^{-}$-I molecules under study. It is well-known that, on a molecule, the LUMO density location is associated with the most favorable sites that shall undergo a nucleophilic substitution.[37,38] Further, in accordance with the Lewis theory for acids and bases this sort of site corresponds to an acidic one.

From Figure 6a it can be observed that, for the fully protonated dopamine molecule, $H_3DA^{+}$, the highest molecular coefficients for the LUMO are located in the amino group; therefore, this indicates also that this is the most probable deprotonation site for this molecule, according to reaction 10. This is in agreement with our previous results of PA, relative energy, Mulliken charges, and bond distances shown above.

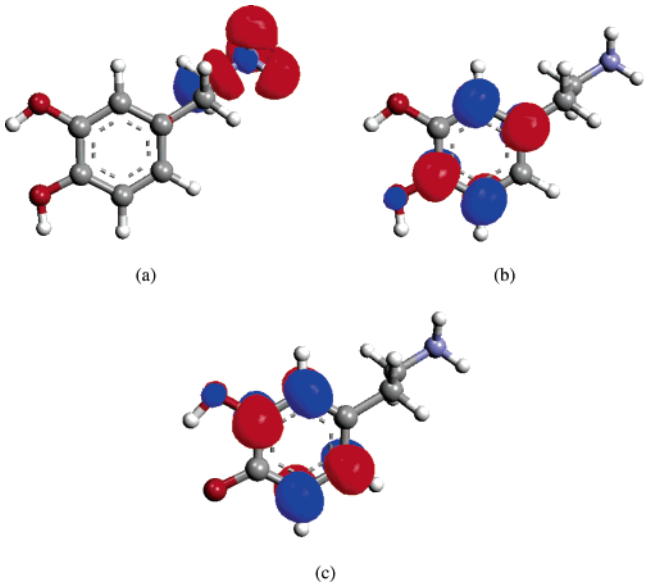


**Figure 6.** LUMO density surface (AM1) for $H_3DA^{+}$ (a), $H_2DA$-I (b), and $HDA^{-}$-I (c). The isodensity value is 0.05 au.

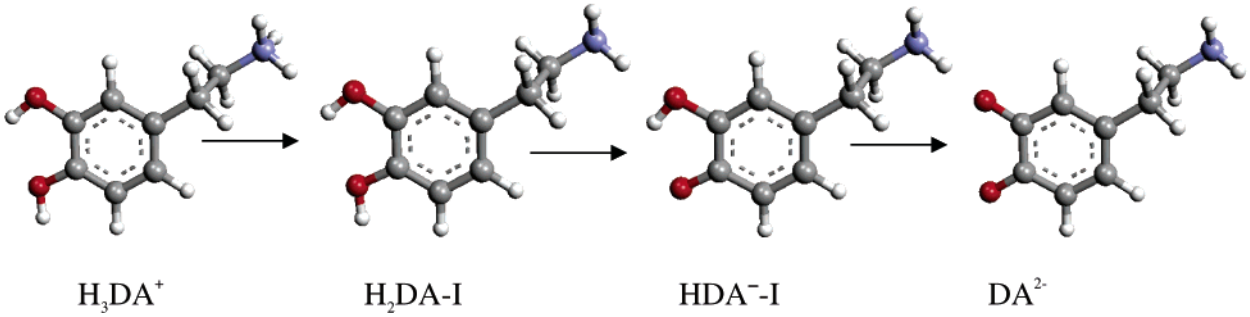


**Figure 7.** Minimum energy geometries of the structures that undergo preferential deprotonation in DA.

Figure 6b shows the LUMO density surface for the $H_2DA$-I molecule, considering that the first proton of the fully protonated form, $H_3DA^+$, was lost from the amino group. From this figure it is possible to note that the highest molecular coefficients for the LUMO are distributed on the O8 atom and in the aromatic ring, although for the dopamine acidity study the LUMO distribution in the said ring is not quite as meaningful. Consequently, two main outcomes are apparent: the first one is related with the susceptibility of the aromatic ring to undergo a nucleophilic substitution. The second and most important in our case is that, from the two remaining acid protons, the most favorable to be lost first corresponds to H20; see reaction 11. It

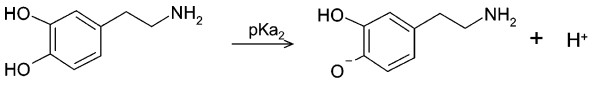


(11)

is important to note that after the loss of the acid protons H20 and H21 the LUMO density surface is located on O7 (see Figure 6c) making H19 the last proton to be lost; see reaction 12.

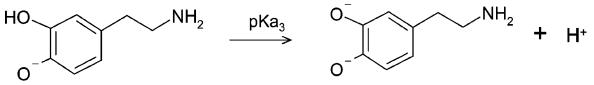


(12)

Our theoretical study performed on the DA molecule, using the different theoretical criteria consider in this work, leads to thinking that DA deprotonation occurs as indicated in Figure 7, that is, first on the $NH_3^+$ group (bound to C9) and then, gradually, on the hydroxyl bound to C6, and finally on the one at the C5 position. Notwithstanding, in order to attain a greater degree of certainty, NMR experiments were performed.

**4.2. Experimental NMR Study.** Experimental NMR spectra were obtained at two pH values, namely, 5.1 and 9.6. In these conditions the predominant dopamine species are $H_3DA^+$ and $H_2DA$, respectively; see Figure 1. The $^{13}C$ spectrum of DA at pH = 5.1 is shown in Figure 8.

The chemical shifts of the carbon atoms in the NMR spectra obtained at different pH values are assigned in Table 11, considering the same numbering system as previously stated for the molecule in Figure 2.

Considering these values and in order to corroborate the deprotonation order obtained by means of the theoretical study, a comparison was made between the experimental and the theoretical $^{13}C$ NMR spectra.

For that purpose, it was necessary to calculate the SCF GIAO magnetic shielding tensor at the B3LYP/6-311+G(*d*,*p*) in a single-point calculation with the minimum energy geometries obtained for the different deprotonation species, calculated also with the same functional and basis set, including the effect of the solvent and a water continuum through the PCM method. The chemical shifts were referred to TMS as indicated previously. With this, the NMR spectrum was created thus obtaining the shifts for all the molecules. Figure 9 shows a comparison of all the shifts for the carbons of the $H_3DA^+$ molecule experimentally and theoretically obtained.

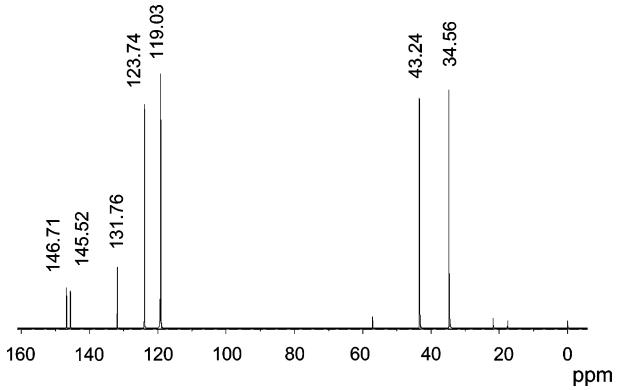


**Figure 8.** $^{13}C$ NMR spectrum of dopamine in $D_2O$ at pH 5.1.

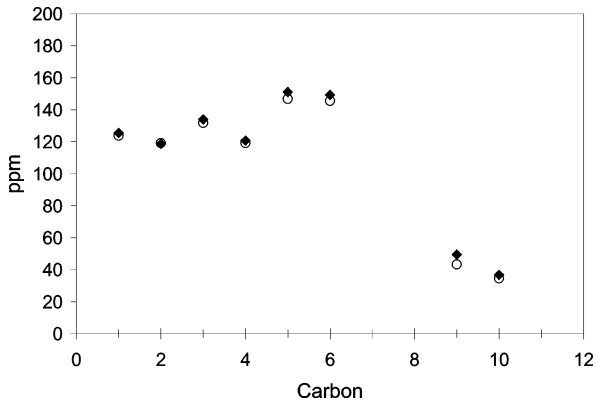


**Figure 9.** Comparison of the chemical shifts of the carbons of the $H_3DA^+$ species: (◆) theoretical (TMS-B3LYP/6-311+G(*d*,*p*)-GIAO); (○) experimental.

As can be observed from Figure 9, the theoretical and the experimental data almost completely overlap for every single carbon atom of the molecule. Such behavior indicates that the calculation used for the $H_3DA^+$ chemical species fully agrees with the experimental data of the DA molecule at this pH.

For the $H_2DA$, the experimental results (see Table 12) of the chemical shifts were used and compared with those, theoretically calculated, corresponding to its three possible isomeric chemical species, namely, $H_2DA$-I, $H_2DA$-II, and $H_2DA$-III; see Figure 7. Figure 10 shows such a comparison.

The analysis of the data depicted in Figure 10 shows that the experimental data are represented better by the theoretical chemical shifts of the $H_2DA$-I isomer. It is straightforward to mention that the matching among the theoretical and experimental chemical shifts of C5 and C6, which are the ones directly

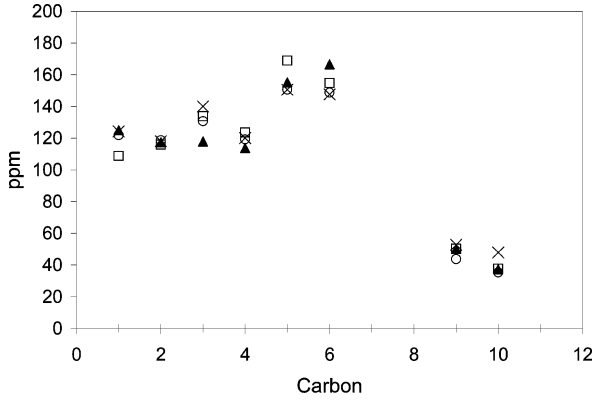


**Figure 10.** Comparison of the theoretical (TMS-B3LYP/6-311+G(*d*,*p*)-GIAO) and experimental shifts for the carbons of the different species of the $H_2DA$. (○) experimental data, (×) $H_2DA$-I, (□) $H_2DA$-II, and (▲) $H_2DA$-III.

**TABLE 12: Experimental Chemical Shifts in ppm of the Carbon Atoms in DA at Different pH Values, Obtained from $^{13}C$ NMR Spectra**

| carbon | pH = 5.1 $H_3DA^+$ | pH = 9.6 $H_2DA$ |
|---|---|---|
| 1 | 123.74 | 121.87 |
| 2 | 119.03 | 118.65 |
| 3 | 131.76 | 130.69 |
| 4 | 119.03 | 119.22 |
| 5 | 146.71 | 150.52 |
| 6 | 145.52 | 148.68 |
| 9 | 43.24 | 43.65 |
| 10 | 34.56 | 35.23 |

linked to the hydroxyls, particularly agrees. However, those others obtained for the $H_2DA$-II and $H_2DA$-III seem to drift apart more compared to the experimental behavior.

## 5. Conclusions

Based on several theoretical criteria, namely, the PA, the energetic stability of the conformers resulting from deprotonation, LUMO distribution, Mulliken charge, and bond distance, we have proposed the deprotonation order for N-protonated dopamine. The deprotonation mechanism proposed was experimentally supported by a good agreement between NMR chemical shifts theoretically calculated by the GIAO method and the $^{13}C$ NMR experimental spectra.

**Acknowledgment.** The authors thank CONACYT for the funding given through Projects 46124 and 48854, GRP for the support given throughout the Retention Program 2005, Exp. 7512/050381, SCA (164699), and GAA (184930) for the studentship received. The authors thank the Materials Department (UAM-A) through Projects 2260220 and 2260231. G.R.P., A.R.H., M.T.R.S., M.R.R., and M.P.P. thank the SNI for the distinction of their membership and the stipend received. The authors are indebted to the Departamento de Química at CINVESTAV México, especially to Professor Alberto Vela, for allowing us to use its data processing facilities. We also express our gratitude to the anonymous reviewers of this paper for their criticisms and suggestions that contributed to the improvement our work.

## References and Notes

(1) Choi, H. J.; Kim, S. W.; Lee, S. Y.; Hwang, O. *J. Neurochem.* **2003**, *86*, 143.

(2) Pezzela, A.; d'Ischia, M.; Napolitano, A.; Misurata, G; Prota, G. *J. Med. Chem.* **1997**, *40*, 221.

(3) Solmajer, P.; Kocjan, D.; Solmajer, T. *Z. Naturforsch.* **1983**, *38c*, 758.

(4) Cooper, J. R.; Bloom, F. E.; Roth, R. H. *The Biochemical Basis of Neuropharmacology*; Oxford University Press: New York, 1986.

(5) Sánchez-Rivera, A. E.; Corona-Avendaño, S.; Alarcón-Angeles, G.; Rojas-Henández, A.; Ramírez-Silva, M. T.; Romero-Romo, M. A. *Spectrochim. Acta, Part A* **2003**, *59*, 3193.

(6) Gerard, C.; Chehhal, H. *Polyhedron* **1994**, *13*, 591.

(7) Sedeh, F.; Ohman, L. O. *J. Inorg. Biochem.* **1993**, *50*, 119.

(8) Kiss, T.; Martin, B. *J. Am. Chem. Soc.* **1989**, *111*, 3611.

(9) Kiss, T.; Gergely, A. *Inorg. Chim. Acta* **1979**, *36*, 31.

(10) Kuznar, B. G.; Weber, O. A. *J. Inorg. Nucl. Chem.* **1974**, *36*, 2151.

(11) Hancock, R.; Orszulik, S. *Polyhedron* **1982**, *1*, 313.

(12) Manjula, V.; Bhattacharya, P. *J. Inorg. Biochem.* **1991**, *41*, 63.

(13) Balla, J.; Kiss, T.; Jameson, R. *Inorg. Chem.* **1992**, *31*, 58.

(14) Porzsolt, E.; Beck, M.; Bitto, A. *Inorg. Chim. Acta* **1976**, *19*, 173.

(15) Hancock, R.; Nakani, B.; Marsicano, F. *Inorg. Chem.* **1983**, *22*, 2531.

(16) Jameson, R. F.; Hunter, G.; Kiss, T. *J. Chem. Soc., Perkin. Trans.2* **1980**, 1105.

(17) Rajan, K. S.; Davis, J. M.; Colburn, R. W. *J. Neurochem.* **1971**, *18*, 345.

(18) Kier, L. B. *J. Theor. Biol.* **1973**, *40*, 211.

(19) Katz, R.; Hellen, S. R.; Jacobson, A. E. *Mol. Pharmacol.* **1973**, *9*, 486.

(20) Pullman, B.; Berthold, H.; Courriere, P. *Int. J. Quantum Chem.* **1974**, *1*, 93.

(21) Grol, C. J.; Rollema, H. *J. Pharm. Pharmacol.* **1977**, *29*, 153.

(22) Cramer, C. J.; Truhlar, D. G. *QCPE Bull.* **1991**, *11*, 57.

(23) Nagy, P. I.; Alagona, G.; Ghio. C. *J. Am. Chem. Soc.* **1999**, *121*, 4804.

(24) Aliste, M. P. *J. Mol. Struct.(THEOCHEM)* **2000**, *507*, 1−10.

(25) Urban, J. J.; Cramer, C. J.; Famini, G. R. *J. Am. Chem. Soc.* **1992**, *114*, 8226.

(26) Alagona, G.; Ghio, C. *Chem. Phys.* **1996**, *204*, 239.

(27) Parr, R. G.; Yang, W. *Density-Functional Theory of Atoms and Molecules*; Oxford University Press: Oxford, 1989.

(28) (a) Becke, A. D. *J. Chem. Phys.* **1993**, *98*, 5648. (b) Lee, C.; Yang, W.; Parr, R. G. *Phys. Rev. B* **1988**, *37*, 785.

(29) Miertus, S.; Scrocco, E.; Tomasi, J. *Chem. Phys.* **1981**, *55*, 117.

(30) Barone, V.; Cossi, M.; Mennucci, B.; Tomasi, J. *J. Chem. Phys.* **1997**, *107*, 3210.

(31) Russo, N.; Toscano, M.; Grand, A.; Mineva, T. *J. Phys. Chem. A* **2000**, *104*, 4017.

(32) Dewar, M. J. S.; Zoebisch, E. G.; Healy, E. F. *J. Am. Chem. Soc.* **1985**, *107*, 3902

(33) Wolinski, K.; Hilton, J. F.; Pulay, P. *J. Am. Chem. Soc.* **1990**, *112*, 8251.

(34) Frisch, M. J.; Trucks, G. W.; Schlegel, H. B.; Scuseria, G. E.; Robb, M. A.; Cheeseman, J. R.; Montgomery, J. A., Jr.; Vreven, T.; Kudin, K. N.; Burant, J. C.; Millam, J. M.; Iyengar, S. S.; Tomasi, J.; Barone, V.; Mennucci, B.; Cossi, M.; Scalmani, G.; Rega, N.; Petersson, G. A.; Nakatsuji, H.; Hada, M.; Ehara, M.; Toyota, K.; Fukuda, R.; Hasegawa, J.; Ishida, M.; Nakajima, T.; Honda, Y.; Kitao, O.; Nakai, H.; Klene, M.; Li, X.; Knox, J. E.; Hratchian, H. P.; Cross, J. B.; Adamo, C.; Jaramillo, J.; Gomperts, R.; Stratmann, R. E.; Yazyev, O.; Austin, A. J.; Cammi, R.; Pomelli, C.; Ochterski, J. W.; Ayala, P. Y.; Morokuma, K.; Voth, G. A.; Salvador, P.; Dannenberg, J. J.; Zakrzewski, V. G.; Dapprich, S.; Daniels, A. D.; Strain, M. C.; Farkas, O.; Malick, D. K.; Rabuck, A. D.; Raghavachari, K.; Foresman, J. B.; Ortiz, J. V.; Cui, Q.; Baboul, A. G.; Clifford, S.; Cioslowski, J.; Stefanov, B. B.; Liu, G.; Liashenko, A.; Piskorz, P.; Komaromi, I.; Martin, R. L.; Fox, D. J.; Keith, T.; Al-Laham, M. A.; Peng, C. Y.; Nanayakkara, A.; Challacombe, M.; Gill, P. M. W.; Johnson, B.; Chen, W.; Wong, M. W.; Gonzalez, C.; Pople, J. A. *Gaussian 03*, Revision B.3; Gaussian, Inc.: Pittsburgh, PA, 2003.

(35) *GaussView 3.0*; Gaussian Inc.: Pittsburgh, PA, 2003.

(36) *ArgusLab 4.0.1*; Mark A. Thompson Planaria Software LLC: Seattle, WA, 2004.

(37) Pearson, R. G. *Chemical Hardness*; Wiley-VCH: Great Britain, 1997.

(38) Fleming, I. *Frontier Orbital and Organic Chemical Reaction*; Wiley and Sons: New York, 1976.

(39) Gómez, B.; Likhanova, N. V.; Dominguez-Aguilar, M. A.; Martinez-Palou, R.; Vela, A.; Gázquez, J. L. *J. Phys. Chem. B* **2006**, *110*, 8928.